Int J Adv Manuf Technol (2015) 77:1057–1070
DOI 10.1007/s00170-014-6536-6

ORIGINAL ARTICLE

Scratching of copper with rough surfaces conducted by diamond tip simulated using molecular dynamics

Jia Li · Qihong Fang · Youwen Liu · Liangchi Zhang

Received: 14 May 2014 / Accepted: 20 October 2014 / Published online: 1 November 2014

Abstract The process of material removal of single crystal copper with rough surfaces subjected to nanoscale scratching is studied in the present paper. We explore the key material removal mechanism by means of the observed variation of material removal under different surface roughnesses, tool speeds, scratching directions, tip shapes, feeds, double tip, and single tip. The investigation reveals that a higher peak on the surface reduces the local area roughness, and a higher valley enhances the stability of surface structure. The plastic deformation by means of dislocation loop transfers from the surface of substrate to the interior of workpiece with the rough or smooth surface during scratching process. A higher scratching velocity results in the increasing surface smoothness and reducing the impact on the rough surface atoms. The scratching along the critical angle 45° between scratching direction and surface texture orientation makes the surrounding atoms produce the minimal variation structure, helps to improve the structural stability, and plays an important role in protecting the scratching surface. The double-tip and single-tip scratching under different scratching feeds makes the rough surface perpendicular to the scratching direction substantially covered by chips or side flow. For different tip shapes, a cone diamond tip causes less plastic deformation in the subsurface than a prismatic diamond tip due to using different diamond tips with a contact area unequal.

Keywords Rough surface · Nanoscale · Scratching · Molecular dynamics · Removal mechanism

1 Introduction

The rapid development of micro/nanoscale electromechanical systems (MEMS/NEMS) has demanded the miniaturized components of nanoscale accuracy [1, 2]. The surface feature production of such components presents significant challenges to understanding the machining mechanisms required for the machining design. However, the nanoscale surface roughness affects the components of accuracy owning to the machining process induced the adhesive and frictional forces [3–5]. In micro/nano mechanical machining, such as cutting and grinding, the adhesion contribution to friction can no longer be neglected because of the large surface area-to-volume ratio of structures and the increasing surface smoothness [6]. Therefore, a fundamental understanding of adhesive and frictional behaviors on a nanoscale-level mechanical process is of great scientific and technological significance [7, 8].

Study of the rough surfaces is of fundamental importance in an improved understanding of the friction and wear between workpiece and tool. Since in reality all engineering surfaces are rough to some degree, the modeling of the contact between these rough surfaces is very important. Under the rough surfaces together, only the peaks or asperities on the surface are in contact and carry very high loads, which cause yielding in the vicinity surface of the materials [9, 10].

In the literature, investigations on mechanical process have been mostly associated with theoretical modeling and molecular dynamics (MD) simulations, which are widely used to solve practical problems, such as nanoparticles [11],

J. Li · Q. Fang · Y. Liu
State Key Laboratory of Advanced Design and Manufacturing for Vehicle Body, Hunan University, Changsha 410082, Hunan Province, People's Republic of China

J. Li · Q. Fang (✉) · Y. Liu
College of Mechanical and Vehicle Engineering, Hunan University, Changsha 410082, Hunan Province, People's Republic of China
e-mail: fangqh1327@hnu.edu.cn

L. Zhang
School of Mechanical and Manufacturing Engineering, The University of New South Wales, Sydney NSW 2052, Australia

nanowires [12–15], and nanofilm [16]. For example, Zhang and Tanaka [17] investigated the deformation mechanisms of copper under the contact sliding with a diamond tip, and they showed that the material removal can take place only when the depth of cut reaches a critical value. Sun and Cheng [18] performed the nanoscale cutting of single crystal aluminum using a quasicontinuum (QC)-based multiscale simulation method. Zhu et al. [19] studied the nanoindentation and nanoscratching of single crystal copper using 3D multiscale method coupling MD and finite element (FE) analysis. Similarly, Chen et al. [20] conducted a systematic study of surface topography in the potassium dihydrogen phosphate (KDP) crystal fly cutting process through multiscale surface simulation. Tong et al. [21] simulated a single-tip and a multi-tip nanoscale diamond tool scratching on copper workpiece using MD simulation. They observed that the diamond multi-tip tool might be more applicable than the single-tip tool. The similar conclusions have been obtained by Tong et al. [22] in a study on nanometric cutting of copper using nanoscale diamond tools. Xu and Zhang [23] investigated the material removal mechanisms and the mechanics behind the vibration-assisted cutting of unidirectional fiber-reinforced polymer composites through a comprehensive analysis. Ji et al. [24] examined the friction behaviors in the interface between the tool and chip interface during the nanometric cutting of a single crystal copper. Han and Gan [25] pointed that the surface planarization realized by the mechanical effect depending on the tribology behavior of nanoparticles is observed by MD simulation techniques during the chemical mechanical planarization. Alao and Konneh [26] reported that precision grinding can be used to generate massive ductile surfaces on silicon so that the polishing time can be reduced immensely and surface quality improved. Zhang et al. suggested a model of grinding hard–brittle silicon wafers [27] and soft–brittle mercury cadmium telluride [28, 29] as well as crystalline nanoparticles of silicon [30] by experimental method using an ultrafine diamond wheel. They showed that the employment of ultrafine abrasive wheels with a hybrid bond material is important to reduce subsurface damage and the cycle time and cost of subsequent polishing process. Zhang and his coauthors [31, 32] discussed through a systematic experimental investigation into the surface integrity of polycrystalline diamond composites (PCDCs) generated by an efficient abrasive-free dynamic friction polishing. Recently, Li et al. [33] investigated the mechanisms of subsurface damage and material removal of monocrystalline copper under a nanoscale high-speed grinding of a diamond tip, found that the transition of deformation mechanisms depends on the competition between the dislocations and deformation twinning, and showed that the Shockley dislocation emission is most likely to occur with the crystal orientations of (0 0 1) [1 0 0] at the angle 45° by the established analytical model. Unfortunately, the traditional simple empirical laws of mechanical process on surface geometry do not always hold effective for or applicable to a micro/nanoscale process due to high surface-to-volume ratio and the greater importance of surface roughness. Thus, the conventional nanoscale scratching models without considering rough surfaces are not always adequate. The following work attempts to provide a more accurate model and also a clearer understanding of material removal of rough surfaces under nanoscale scratching.

The purpose of this paper is to build up an actual model for the mechanism of material removal on single crystal copper workpiece with rough surfaces under nanoscale scratching with the aid of MD analysis. The effects of nanoscale surface roughnesses, tool speeds, scratching directions, double tip and single tip, feeds, shape of the tip on the variation of the surface integrity of ground surface, temperature, and scratching forces will be performed with the single crystal copper with rough surfaces subjected to nanoscale scratching.

2 Simulation method

The MD simulation model of nanoscale scratching of copper with rough surfaces contains a face-centered cubic (FCC) single-crystal copper workpiece and a rigid diamond scratching tip/tool, as shown in Fig. 1. A peak width is a, valley width b, valley depth c, and depth of cut h, with which the sum of peak width and valley width is equal to a constant value of 1.5 nm. The nanoscale surface roughnesses are defined as the surface roughness factors $R_x=a$ and $R_z=c$, which can be independently and separately analyzed depending on the function of interest. The size of the workpiece is 25.3 nm × 18 nm × 12 nm and three orientations of the workpiece in x-[1 0 0], y-[0 1 0], and z-[0 0 1]. The atoms of copper workpiece are allocated into one of three different zones: boundary atoms, thermostat atoms, and Newtonian atoms. The motions of the thermostat and Newtonian atoms obey the classical second Newton's law. The three layers of the boundary atoms at the left and bottom of the workpiece are kept fixed in space to eliminate the rigid body motion of the workpiece [25, 33]. The next three layers of the atoms adjacent to the boundary ones at the left and bottom of the workpiece are thermostat atoms. The initial workpiece temperature is 293 K. As considerable energy adds to the thermostat atoms during scratching, heat dissipation is carried out during the MD simulation to keep the thermostat atoms at the constant temperature of 293 K, by adjusting the atom velocities at every five computational time steps using the velocity rescaling method. Based on the previous work of MD simulations [34, 35], a periodic boundary condition is maintained along the x and y directions to reduce the effect of the simulation length scale.

The diamond tip/tool created from the perfect diamond atomic lattices has a spherical shape with a radius of 3 nm.

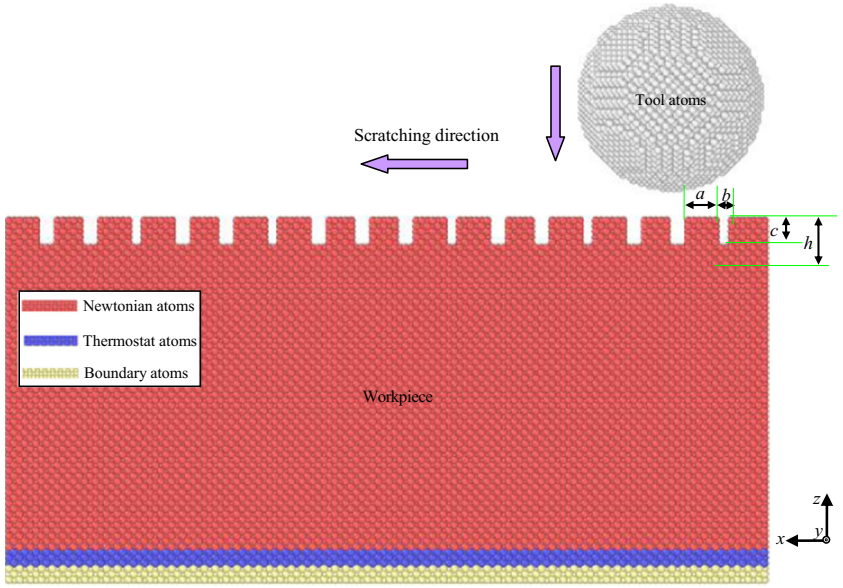

Fig. 1 MD simulation model of a nanoscale scratching copper workpiece with rough surface

Due to much higher hardness of diamond than copper, the tool is treated as a rigid body during the nanoscale scratching process. There are three different atomic interactions in the MD simulation: (1) the interaction between copper atoms (Cu–Cu) in the workpiece, which will be described by the embedded atom method (EAM) potential [33, 36] in our study, as the EAM potential has been found reliable; (2) the interaction between diamond atoms (C–C) in the tool, which will be ignored in the present study as the tool is treated as a rigid body; and (3) the interaction between the workpiece and tool (Cu–C) atoms, which will be depicted by the Morse potential [33, 37, 38]. The parameters for the Morse potential in our simulations are taken as the cohesion energy D= 0.087 eV, the elastic modulus α=5.14 Å^{-1}, and the equilibrium distance between two atoms r_0=2.05 Å according to [33, 37, 38]. The cutoff radius of the Morse potential is chosen to be 9.025 Å [38] to ensure the computational efficiency.

3 Simulation results and discussion

All MD simulations are completed using the classical molecular dynamics package IMD with a time step of 1 fs [39]. The software OVITO is utilized to visualize the MD data and generate the MD snapshots [40]. Our MD scratching simulation consists of three stages: the relaxation stage, the indentation stage, and the scratching stage. Before scratching, we firstly relax the copper workpiece to obtain equilibrium configurations by taking the following steps: the workpieces are first relaxed to their minimum energy configurations at 293 K using the Nose–Hoover thermostat. Then, the equilibrated workpieces are subjected to scratching by using a spherical tool in the microcanonical ensemble (NVE). The scratching process involves an initial penetration and subsequent scratching. The tool firstly penetrates into the surface of copper workpieces along the negative z direction at a constant velocity of 20 m s^{-1} until it reaches the pre-determined penetration depth of 1 nm [41]. Lastly, it scratches along the [1 0 0] direction on the (0 0 1) surface of the workpiece at a constant velocity of 30 m s^{-1}. Table 1 summarizes the main computational parameters used in the MD simulations for reference.

3.1 Effect of nanoscale surface roughness

To investigate nanoscale scratching monocrystalline copper with rough surfaces, a series of simulations are performed and atoms are colored according to their heights out of the original surface. The rough surface with a deterministic pattern in the peak and valley regions introduces new issues in nanometer scratching for studying surface characterization, with which existing experiment works little analyses due to the limitations of the current real-time detection equipment. Here, new MD simulations are considered allowing the adjustment and settings of the functional features composing the shape of rough surface. The top partial views of the scratching surface of the

Table 1 Computational parameters used in the MD simulations

Materials	Workpiece: copper	Tool: diamond
Dimensions	25.3 nm×18 nm×12 nm	Radius 3 nm
Number of atoms	469,000	19,955
Time step	1 fs	
Initial temperature	293 K	
Scratching velocity	30, 50, 100, and 200 m s^{-1}	
Depth of cut	1 nm	
Scratching distance	0–20 nm	
Scratching direction	[1 0 0] on (0 0 1) surface	

specimen with different surface roughness factors R_x and R_z are shown in Fig. 2a–d and 2e–h, respectively. Figure 2 shows that as the surface roughness factor R_x rises, a volume of the surface pileups increases as well. For the surface roughness factor R_z, there is a contrary result that a larger surface roughness factor R_z reduces a volume of the surface pileups. It is known that the accumulation of surface steps produces the material pileup, accompanying dislocations nucleating gliding and terminating at the surface [42]. A larger surface roughness factor R_x accelerates the reduction of the local area roughness due to the fact that it improves the diffusion of surface atomics, fills the low-lying region, and reduces the partial protrusion owing to the shear stress dispersed by the surface roughness factor R_x. Moreover, when the surface roughness factor R_x is 1 nm, this effect becomes extremely strong on scratching surface. For different surface roughness factors R_z, the scratching surface with a smaller surface roughness factor R_z suffers from the surface deformation that the layers of Newtonian atoms subjected to scratching force will shrink or swell on the rough surface of the workpiece. The scratching force passes through the surface atoms and depends upon the surface roughness factor R_z. Although a larger value of surface roughness factor R_z shows a natural obstacle of atomic diffusion between two rectangular textures, it is at all possible to protect surface structure from the scratching force. On the other hand, the rough surface can store wear particles and has a positive effect on reducing the abrasion of the tool.

Figure 3 illustrates MD simulations of dislocation loops taken with a reflection of [1 1 $\bar{1}$] at different surface roughness factors R_x during the diamond tool scratching. The lattice defects are identified by the common neighbor analysis (CNA) [43]. Similar results have been reported by experimental methods [44] and MD simulations [45] for prismatic dislocation loops, which is made up primarily of four stacking

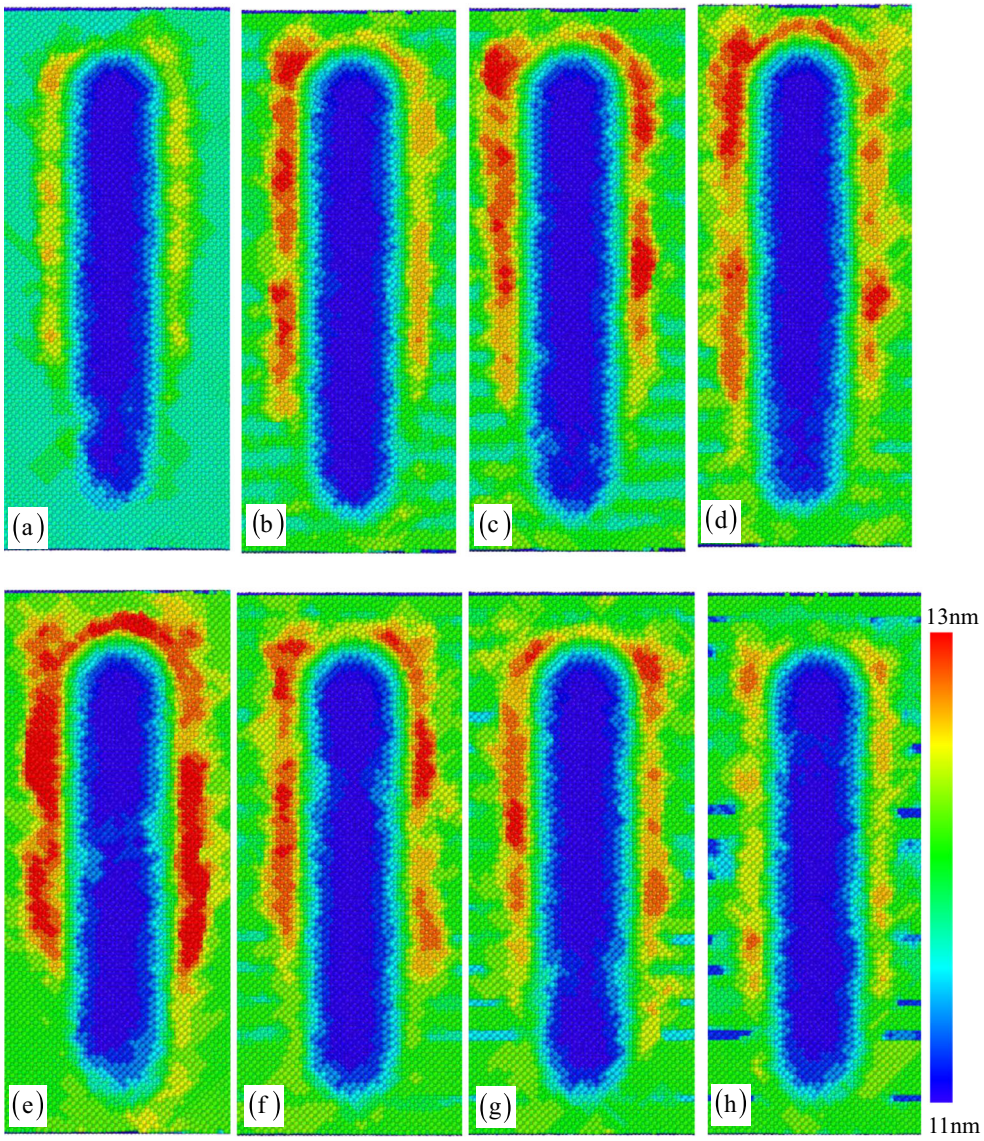

Fig. 2 The top partial views of scratching surface. The surface roughness factors R_x are **a** 0 nm, **b** 0.5 nm, **c** 0.7 nm, and **d** 1 nm. (The scratching distance and surface roughness factor R_z are 20 nm and 0.3 nm, respectively.) The surface roughness factors R_z are **e** 0 nm, **f** 0.3 nm, **g** 0.5 nm, and **h** 0.8 nm. (The scratching distance and surface roughness factor R_x are 20 nm and 1 nm, respectively.)

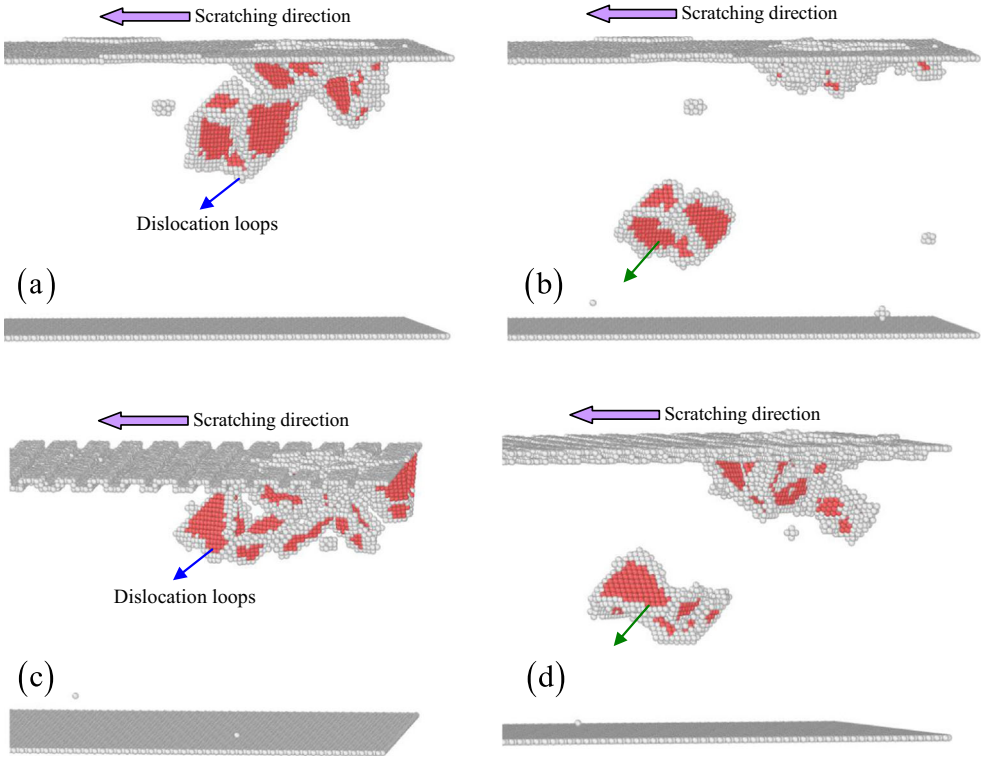

Fig. 3 The side partial views of the lattice defects during the scratching process at the scratching process distance: **a**, **c** 4 nm and **b**, **d** 8 nm. (The surface roughness factor R_x is 0 nm in **a**, **b** and 0.7 nm in **c**, **d**. Atoms are colored according to the calculated CNA values: ISF (*red*) and partial dislocation and surface atoms (*white*). FCC atoms are excluded for a clearer visualization of the defect structures.)

fault planes in {111} plane, each stacking fault plane consisting of two partial dislocations sandwiching a stacking fault zone in Fig. 3. Dislocation loops emit into the workpiece material, corresponding to the deformation by means of dislocation loop transfers the interior of workpiece material to release the plastic deformation beneath the tool to improve the stability of the materials beneath the tool. This phenomenon clearly explains the behavior of plastic flow during scratching rough surface workpiece. The effect of surface roughness also affects the shape and position of dislocation loops, which reduces the accumulated scratching energy corresponding to the temporary drop of the scratching force. The results on the plastic deformation and dislocation mechanism has a great benefit to enhance understanding of the surface roughness effect during nanoscale scratching process for the reasonable selection of machining parameters.

The variations of the average temperature and the scratching forces with different surface roughness factors R_x and R_z are showed in Figs. 4 and 5, respectively. A comparison of Fig. 4a, b shows that the average temperature increases with the increment of the scratching distance, and the effect of surface roughness factor R_x more strongly affects on the temperature than the effect of surface roughness factor R_z. F_x and F_z represent the average tangential and normal scratching forces, respectively, which are obtained by summing the atomic forces of workpiece atoms on tip atoms during the scratching process. Both the tangential and normal scratching forces increase with the increasing surface roughness factor R_x, but decrease with the increasing surface roughness factor R_z. As can be seen from Fig. 4, the larger surface roughness factor R_x and the smaller surface roughness factor R_z produce more chips requiring the larger forces to complete this process. In addition, the average scratching forces are strongly affected due to the effect of the surface roughness factor R_z than due to the effect of surface roughness factor R_x. The observed scratching forces on our simulated rough surfaces are similar to the experimental results by Tyrell and Attard [46].

Results for the average friction coefficient of single crystal copper with different surface roughness factors are shown in Fig. 6. The average friction coefficient is defined as the ratio of the average friction force to the average normal force, and the average friction force is considered as the force parallel to the scratching direction. According to the work of Zhu et al. [47], the friction coefficients at nanoscale consist of the ploughing friction coefficient, the adhesion friction coefficient, and the chip component of friction coefficient. It can be seen that the average friction coefficients increase with the increasing surface roughness factor R_x, but decrease with the increasing surface roughness factor R_z. This is considered to be the cause of the scratching on the rough surfaces that produces more chips to lead the chip component of friction coefficient increasing when the surface roughness factor R_x increases or the surface roughness factor R_z decreases.

3.2 Effect of tool speeds

Figure 7 shows the surface morphologies as a result of varying nanoscratching speed, in which the atoms are colored

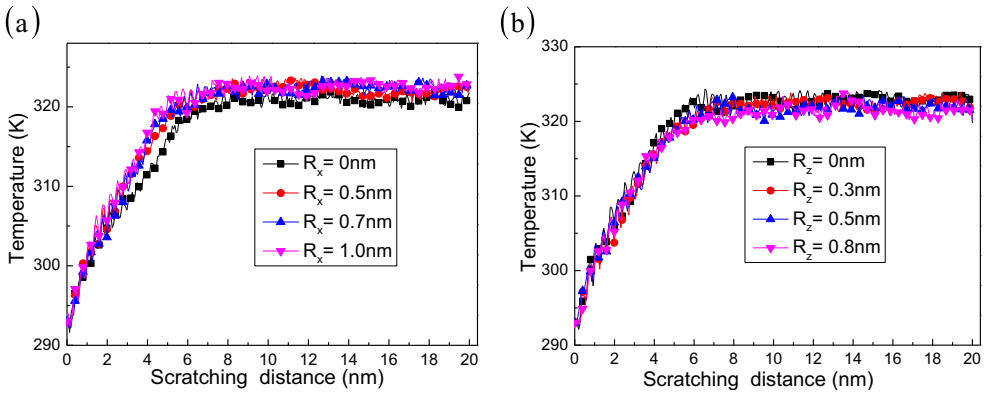

Fig. 4 Variation of the average temperature during scratching monocrystalline copper with surface roughness factor R_x (**a**) and with surface roughness factor R_z (**b**). (The surface roughness factors R_x and R_z are 1 and 0.3 nm, respectively)

according to their heights. It can be seen that a higher scratching velocity obtains a larger volume of the surface pileups. It is known that the chip formation is more pronounced in workpiece with less work hardening [33, 37]. From the above MD simulation, we can conclude that the stronger work hardening in the copper workpiece is caused by the frequent dislocation-ISF interactions. In addition, the dislocations nucleate and glide freely in a single crystalline copper. Figure 7 also demonstrates that the scratching speed has a strong influence on the distribution of the surface pileups. A comparison of Fig. 7a–d shows that the chipping volume in front of the scratching tip increases with the increasing scratching speed, but the volume of the material pileups on the sides of the groove decreases. When the scratching speed is 200 m s^{-1}, however, the above effect becomes trivial, indicating that the material removal rate will reach a critical value as the tool speed increases. These results are consistent with machining smooth copper at nanoscale [33] and show that the smooth or rough surface lightly affects on the material removal of monocrystalline copper. Moreover, a higher speed results in better removing the surface and reducing the impact on the surrounding surface. Especially, this advantage may be more prominent in this case, which machines the local part of the surface.

In the MD simulations, when surface roughness factor R_x and R_z are fixed at 1 and 0.3 nm, the average temperature increases with the increasing scratching speed during the scratching on the rough surface, as shown in Fig. 8a. It can be seen that a higher scratching speed produces a greater temperature with the scratching distance increment because of dramatically accelerating the dislocation nucleation and movement to cause more thermal energy. Additionally, it is clear that the fluctuation increment of the average temperature becomes smoother as the scratching distance increases due to the most heat taken away by chips under a stable scratching process. Figure 8b shows that during scratching on the rough surface, at the low scratching speed, both the tangential and normal scratching forces appear as sharp rising and then at the high scratching speed, the asymptotic behavior approaches a constant. The transition from fast to slow scratching force takes place over a relatively narrow range of speed, which is very sensitive to the scratching speed. It is noted that the stability of rough surface rapidly reduces, and the groove on both sides displays distortions (see, Fig. 7) with the increasing tool speed because a higher scratching speed brings more heat and lager scratching forces.

3.3 Effect of scratching directions

MD simulations of the line-type grooves with different scratching angles (θ—0°, 30°, 45°, 60° and 90°) are also conducted. The scratching angle θ is defined as the angle between the scratching direction and the surface roughness direction (texture orientation) as schematically shown in

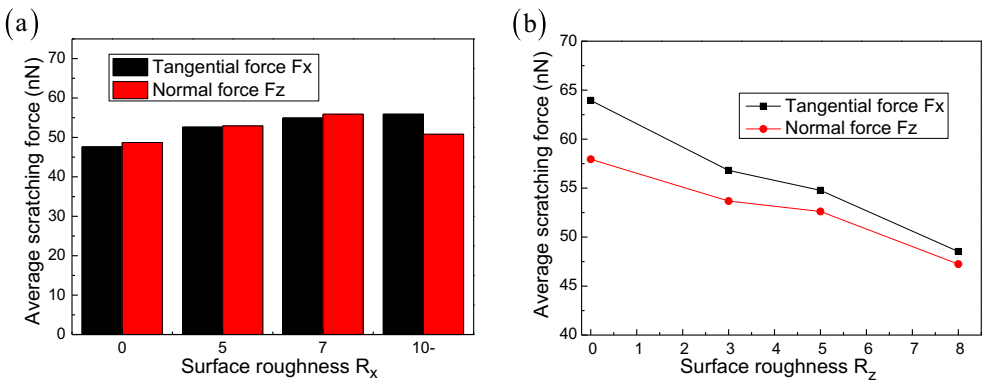

Fig. 5 Variation of the average scratching forces during scratching monocrystalline copper with surface roughness factor R_x (**a**) and R_z (**b**). (The surface roughness factors R_x and R_z are 1 and 0.3 nm, respectively)

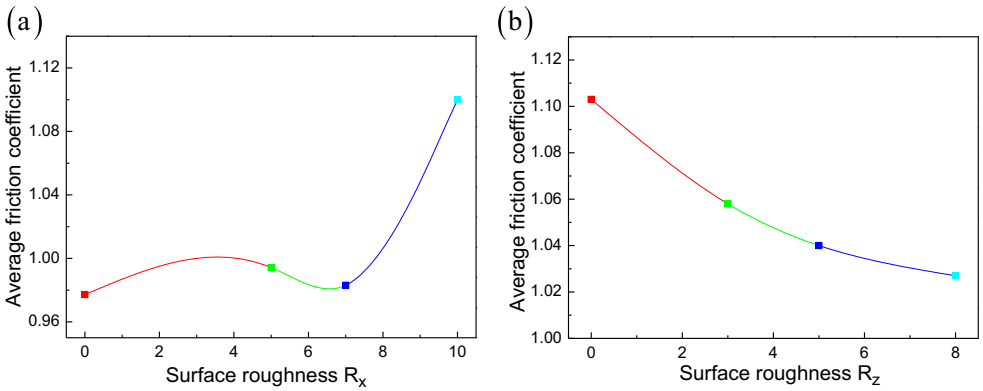

Fig. 6 Relationship between average friction coefficient and surface roughness factors

Fig. 9a. Figure 9b–f presents the chips of the deformed copper workpiece for different scratching angles. The scratching speed with four scratching angles is kept at a constant value of 30 m s^{-1} along the scratching direction. The depth of cut and tool radius are kept as a constant value of 1 and 3 nm, respectively. When the scratching angle is below the critical value of 45°, the chipping volume in front of the tool increases and the volume of material pileup on both sides of the groove decreases. When the scratching angle is above the critical value of 45°, however, the chipping volume in front of the tool decreases and the volume of material pileup on both sides of the groove increases. It seems that with the scratching angle of 45°, the best surface quality of groove can be obtained [33, 38]. The scratching along the scratching angle of 45° makes the surrounding atoms produce a minimal variation structure, helps to improve a structural stability, and plays an important role in protecting the finished surface. Hence, the surface integrity of workpiece during the scratching process strongly depends on the surface roughness direction or the texture orientation, and the effect of the scratching direction.

Figure 10a shows a comparison of the average value of the temperature for these four scratching angles. It can be seen from Fig. 10a that the average temperature at the scratching distance from 5 to 15 nm firstly increases and then keeps relatively stable for different angles. With the increasing scratching angle, the average temperature to the scratching distance curve decreases from 0° to 30°, increases from 30° to 45°, and decreases from 45° to 90°. In addition, a comparison of the scratching angle of 90° and 0° reveals a different trends and values of the average temperature due to the surface roughness direction, although these two scratching processes have the same scratching direction family. The average force *Fg* and normal force *Fz* curves of workpiece under different scratching angles are shown in Fig. 10b. The force $Fg=Fx\cos\theta+Fy\sin\theta$ is defined as along the scratching direction force, in which the average values are defined as the values of force components at the scratching distance from 5 to 15 nm. For different angles between the scratching direction and the surface roughness direction, the average values of the normal force *Fz* are roughly consistent about 35 nN. However, the average values of force *Fg* increase and then decrease with

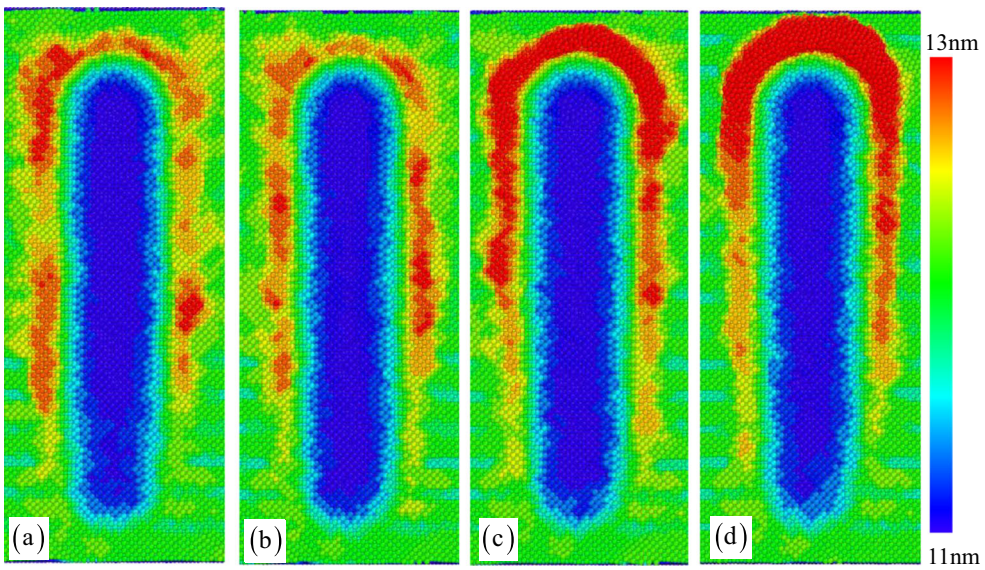

Fig. 7 Variation of surface morphology with the change of scratching speed of **a** 30 m s^{-1}, **b** 50 m s^{-1}, **c** 100 m s^{-1}, and **d** 200 m s^{-1}. (The scratching distance, surface roughness factors R_x and R_z are 20, 1, and 0.3 nm, respectively.)

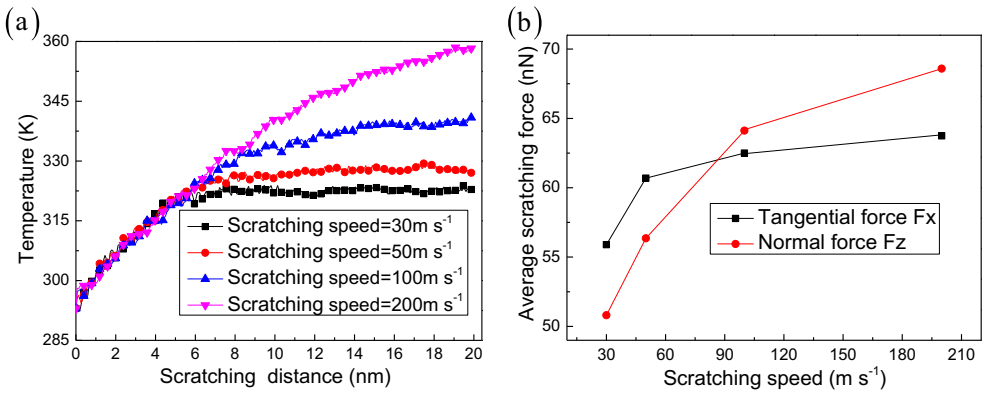

Fig. 8 Effect of scratching speed **a** variation of the average temperature and **b** variations of scratching forces. (The surface roughness factors R_x and R_z are 1 and 0.3 nm, respectively.)

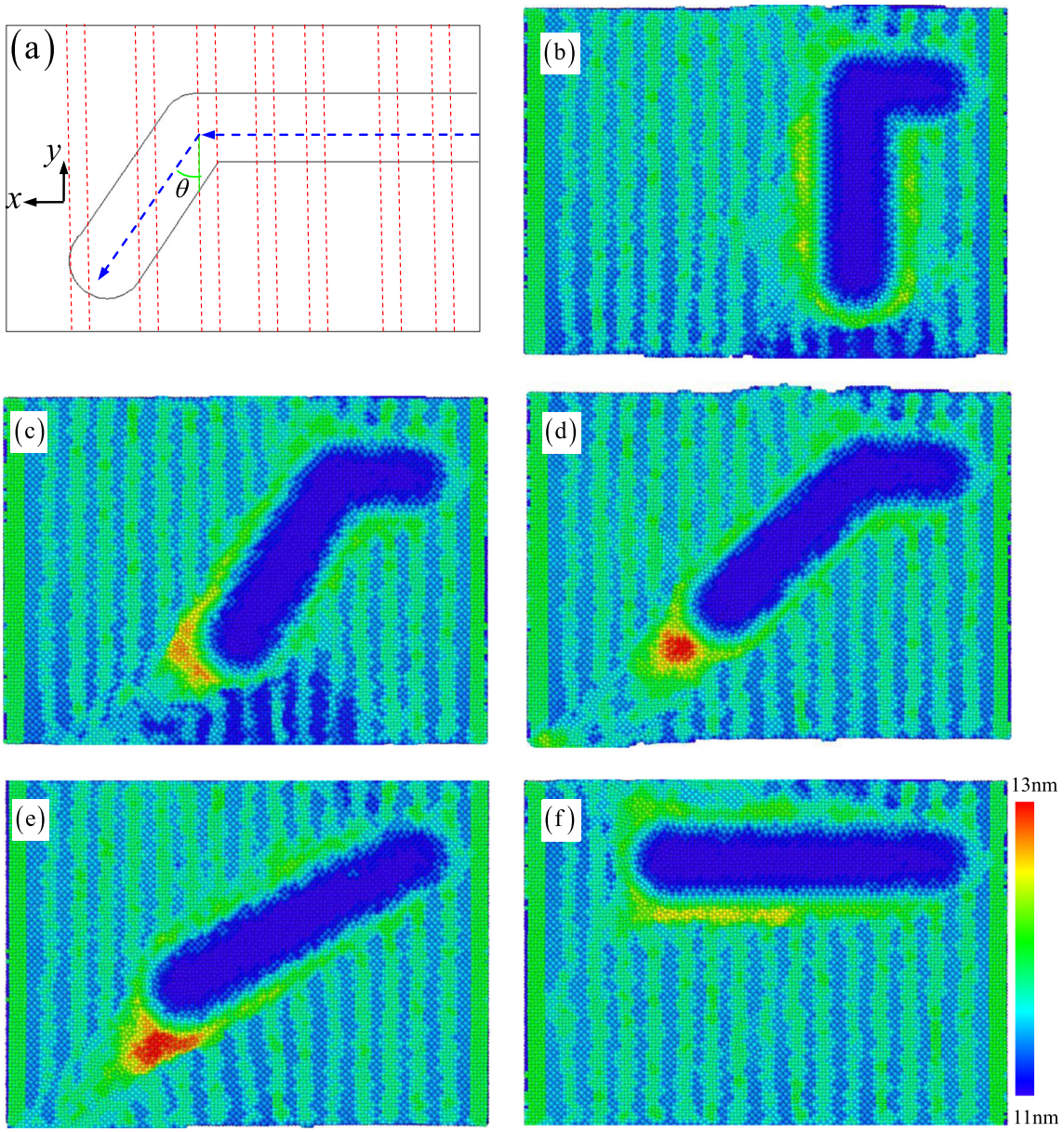

Fig. 9 **a** A schematic illustrating fabrication process for different scratching angles. Illustration of the strategy of studying the effect of scratching directions is **b** 0°, **c** 30°, **d** 45°, **e** 60°, and **f** 90°. (The tool speed and surface roughness factors R_x and R_z are 30 m s^{-1} and 1 and 0.3 nm, respectively. Atoms are colored according to atomic height.)

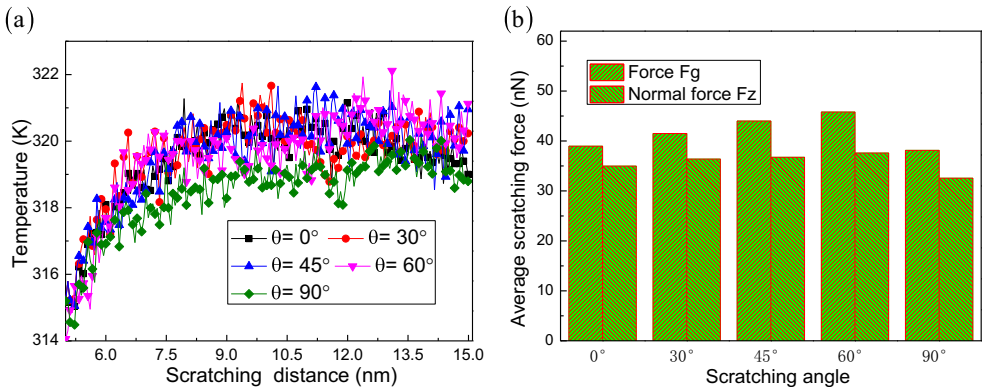

Fig. 10 Effect of the scratching angle. **a** Variations of scratching forces with scratching distance 5–15 nm and **b** variations of average temperature. (The tool speed and surface roughness factors R_x and R_z are 30 m s^{-1} and 1 and 0.3 nm, respectively.)

the increase of the scratching angles. In addition, the force *Fg* rises to its highest amount at the angle of 45° and 60° to the surface roughness direction. Especially, both the force *Fg* and normal force *Fz* at the angle of 90° are the lowest values. This is because the scratching tool just above the valley reduces the material removal under scratching direction with the angle of 90°.

3.4 Effect of double-tip and single-tip scratching

The top view of the scratching surface of the specimen in simulation with double tips and simulation with single tip under different feeds are shown in Fig. 11. In our simulations, the depth of cut is 1 nm and the scratching feeds are 0.5, 1, 1.5, and 2 nm, respectively. With the increasing feed, the volume of the workpiece material pileup at the region between the grooves sharply increases. A comparison of these different scratching processes shows that the chipping volume in front of the tool has a significant change between double-tip and single-tip scratching for different scratching feeds. The double-tip scratching obtains more chipping volume than the single-tip scratching, reduces less the side flow volume, and improves the material removal rate. In the single-tip scratching, the first groove on the right side distorts and the scratching width of first groove narrows. This is because when the second time scratching, due to the lack of material support from the left side, the second time scratching chips move toward the first groove, which leads the first groove to shallow and the middle side flow material to tilt toward the left side. However, in simulation with double tips, two parallel grooves are always obtained on the workpiece surface with different feeds. It also reveals that when the feed decreases down to nanometer range, the second time scratching has a significant influence on the first scratching. Recently, Zhang et al. [48] have reported that when the feed between the first and second grooves is larger than 3.1 nm, two parallel grooves after scratching with double or single tip cause just a little distortion during a cone diamond tip scratching copper. Our results agree with their conclusion and fulfill it by further confirming that this phenomenon happens not only in a sphere-shaped tool tip but also in rough surface. It can be clearly seen that the rough surface perpendicular to the direction of the scratching is substantially covered by chips or side flow, which reveal that the double-tip and single-tip scratching has a significant impact on the surface. Figure 11 also provides some key insights into the differences between the scratching mechanisms associated with the double-tip and single-tip scratching. In addition, a significant improvement in surface roughness is obtained when the double-tip scratching is used.

Figure 12 shows that the average temperature for different feeds slightly changes as the scratching distance increases. The double-tip scratching shows the highest temperatures at the workpiece than the single-tip scratching under different feeds. A high temperature in the scratching zone increases the thermal activation energy, which further accelerates the dislocation nucleation and motion and brings about the hardening and lower plasticity. The beneficial effect of high temperatures by an appropriate coolant may help to reduce surface roughness [49, 50]. Figure 13 shows the variation of the scratching forces for a combination of (0 0 1) [1 0 0] orientation. The forces first decrease, increase, and then keep stable with the increasing scratching distance under the double-tip scratching. It seems that the tangential scratching force remains larger than the normal force for both the double-tip and single-tip scratching during nanoscale scratching process on rough surfaces with different scratching feeds. This means that the tool has a large intrusion action to the workpiece, which causes the generation and evolution of the dislocations [51]. Compared to the conventional scratching, the difference is that the tangential forces over normal forces are attributed to the chip component of friction force [47]. This strongly suggests that the chip-induced scratching forces are independent of the scratching feeds and cannot be neglected for studying nanoscale scratching on the rough surface.

3.5 Effect of tip shape

To analyze different tip shapes impacting on the scratching surface, simulations are performed with a sphere, cone, and prismatic diamond tips, as shown in Fig. 14. The CNA is

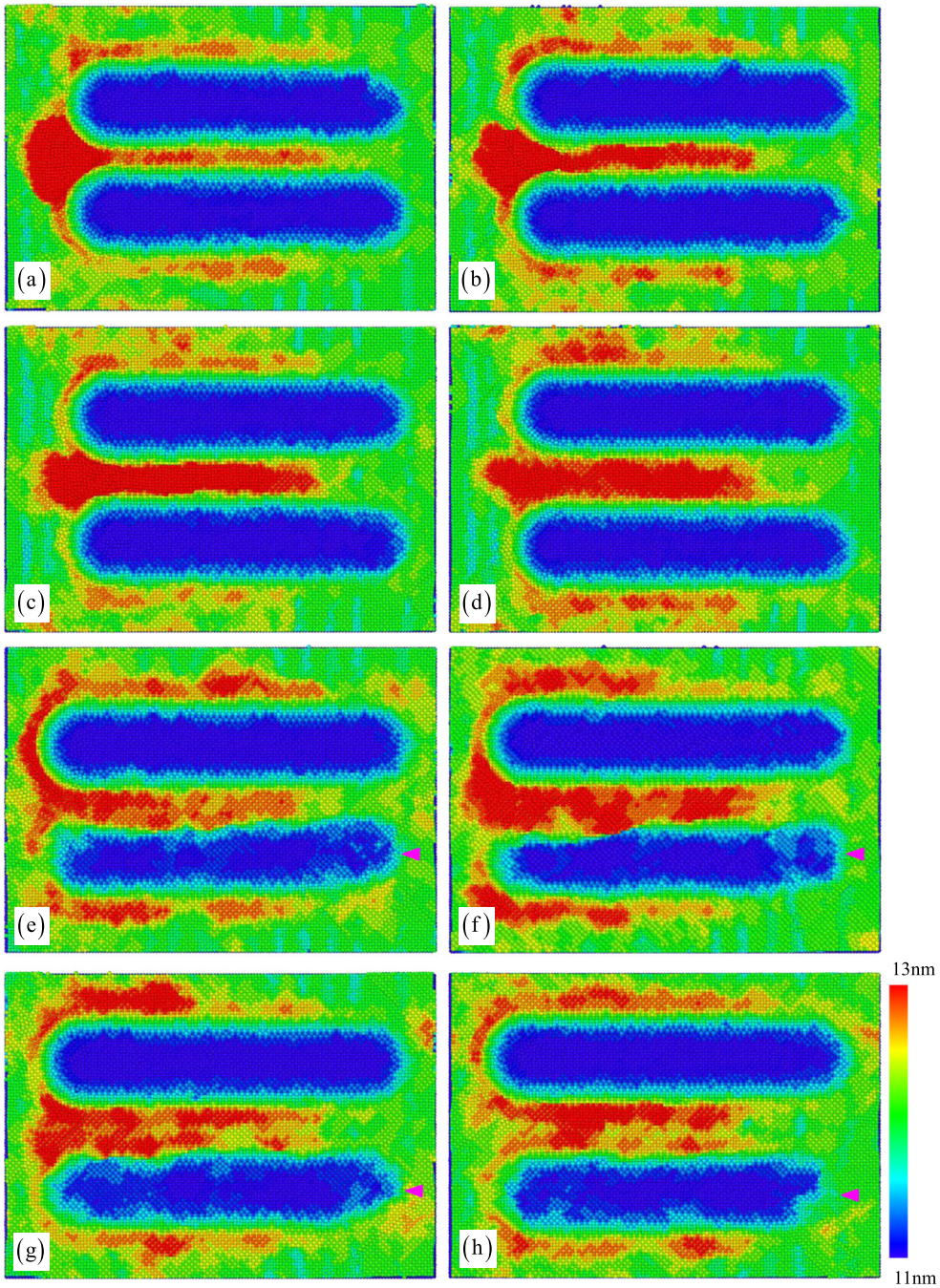

Fig. 11 The top view of scratching surface under double tips for different feeds: **a** 0.5 nm, **b** 1 nm, **c** 1.5 nm, and **d** 2 nm; under single tip for different feeds: **e** 0.5 nm, **f** 1 nm, **g** 1.5 nm, and **h** 2 nm. (The surface roughness factors R_x and R_z are 1 and 0.3 nm, respectively. *Triangle* indicates the first time scratching under single tip)

adopted to identify the feature of each atom before and after deformation during nanoscratching [43]. The difference between ISF and dislocation cores is distinguished. Hence, Fig. 14a–c presents the instantaneous structures of the deformed workpiece under different tip shapes. It can be seen that a prismatic diamond tip generates more ISF atoms in the subsurface and a cone diamond tip less ISF atoms due to scratching using different diamond tips with a contact area unequal. Figure 14d–f shows the resulting surface morphologies of different tip shape combinations of crystal orientation (0 0 1) [1 0 0] and illustrates that scratching is simulated with either the symmetric edge or the larger flat surface of the tip plowing the workpiece. It is seen that a prismatic diamond tip causes more chipping volume and less volume of the workpiece material pileup on both sides of the groove. In addition, the number of the surrounding atoms with structural changes depends on the tip shape in Fig. 14d–f.

Figure 15a shows the variation of average temperature versus the scratching distance for different diamond tips on the copper surface. The prismatic diamond tip generates more heat due to forming more chips. The average temperature tends to stable under different diamond tips, because the heat

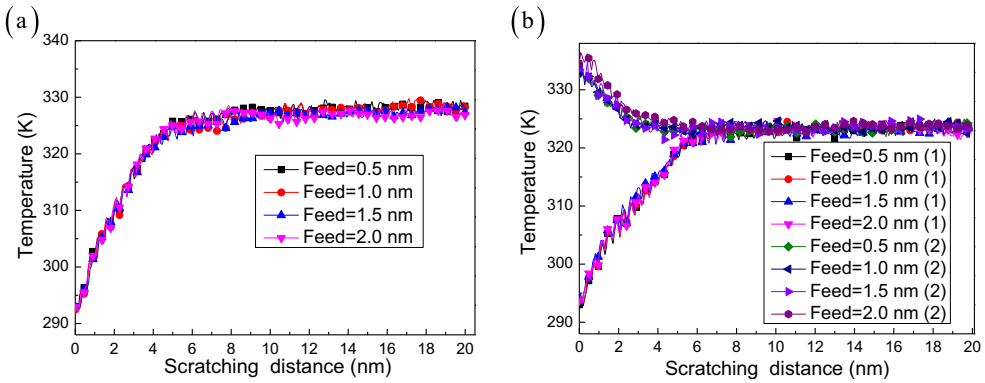

Fig. 12 Comparison of average temperature during nanoscratching process with increasing scratch distance: **a** comparison of average temperature with double tips; **b** comparison of average temperature with single tip. (*1* represents the first time scratching and *2* the second time scratching.)

is carried away by chips and by conduction into the tool and workpiece. As observed with different diamond tips in Fig. 15, both the tangential and normal scratching forces obtained with the diamond tips are the minimum value when the diamond tip is spherical. The tangential scratching force with the prismatic tip reaches a maximum because of forming the larger volume of chip. The normal scratching force with the cone tip obtains the peak compared with the other two shape tips due to the fact that the contact area between the tip and workpiece in the cone tip vicinity is larger than in the sphere or prismatic tip vicinity. It can be seen that the increasing number of workpiece atoms interacting with atoms at the front of the tip intensifies the scratching force and depends on the tip shape.

4 Conclusions

Molecular dynamics simulations of nanoscale scratching are performed with the single crystal copper with rough surfaces to examine the effects of surface roughness, tool speed, scratching direction, shape of tip, feed, double tip, and single tip on the variation of material removal, temperature, and scratching force. Based on the presented results and discussions, the following main conclusions can be drawn.

1) A higher surface roughness factor R_x reduces the local area roughness due to exacerbating the diffusion of surface atomics and filling the low-lying region, and a larger value of surface roughness factor R_z protects the stability of surface structure from the scratching force.
2) As a higher scratching velocity increases, it can cause the surface to better remove and reduce the impact on the surface atoms. These results indicate that a higher scratching velocity results in more chipping volume, larger scratching force, and higher temperature in workpiece are consistent with scratching smooth copper at nanoscale.
3) The scratching along the critical value of the angle 45° between the scratching direction and the surface roughness direction (texture orientation) makes the surrounding atoms produce minimal variation structure, helps to improve structural stability, and plays an important role in protecting the scratching surface.
4) Under different scratching feeds, the double-tip scratching obtains more chipping volume than the single-tip scratching, reduces the side flow volume, and improves the material removal rate, specifically making the rough surface perpendicular to the scratching direction substantially covered by chips or side flow.
5) For different tip shapes, a prismatic diamond tip generates more ISF atoms in the subsurface, and a cone diamond tip brings about less ISF atoms due to scratching using

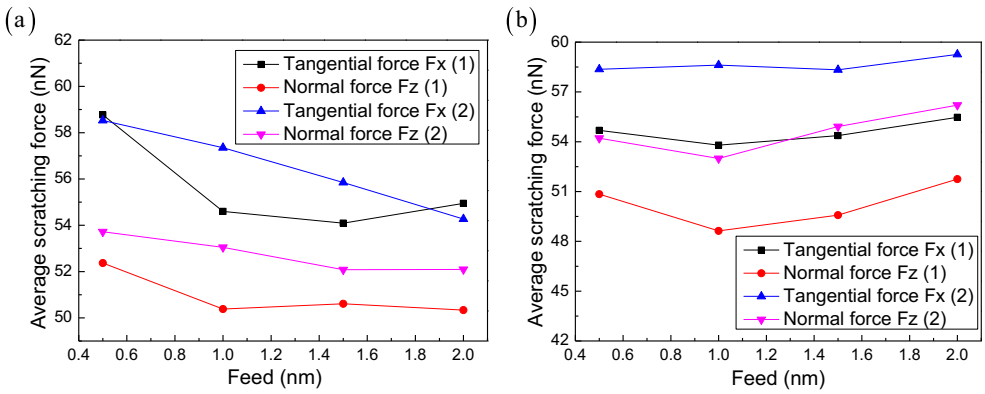

Fig. 13 Comparison of forces during nanoscratching process with different scratching feeds: **a** comparison of forces F_x and F_z with double tips; (*1* represents the first tip and 2 the second tip) **b** comparison of forces F_x and F_z with single tip (*1* represents the first time scratching and 2 the second time scratching)

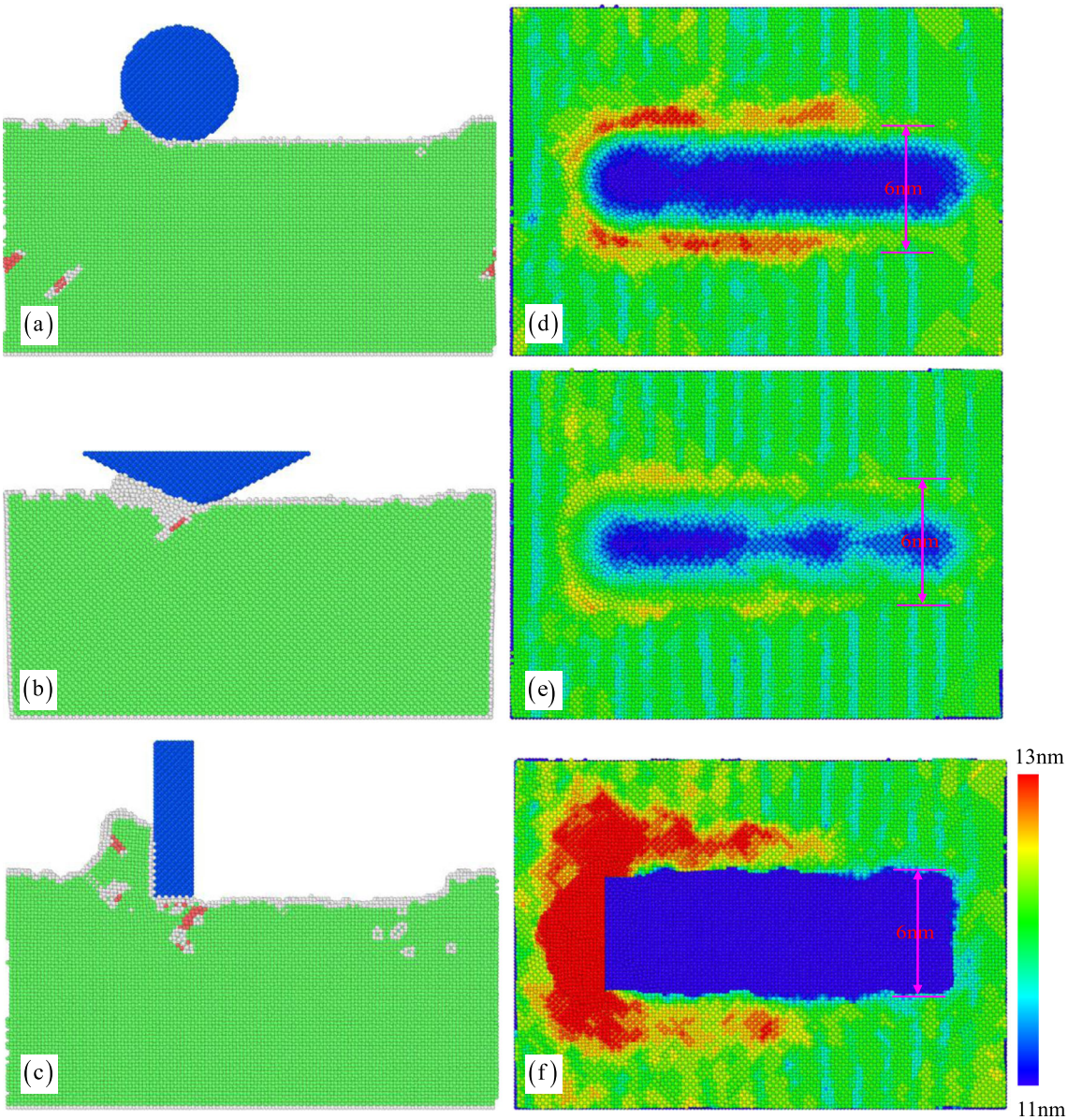

Fig. 14 Illustration of the strategy of studying the effect of tool shape is (**a**, **d**) sphere, (**b**, **e**) cone, and (**c**, **f**) prismatic at the scratching process. (The tool radius, depth of cut, tool speed, and surface roughness factors R_x and R_z are 3 nm, 1 nm, 30 m s^{-1}, and 1 and 0.3 nm, respectively.) **a–c** atoms are colored according to the calculated CNA values (*red*, ISF atoms; *blue*, FCC atoms; *white*, other atoms including surface atoms and dislocation cores) and **d–f** according to atomic height

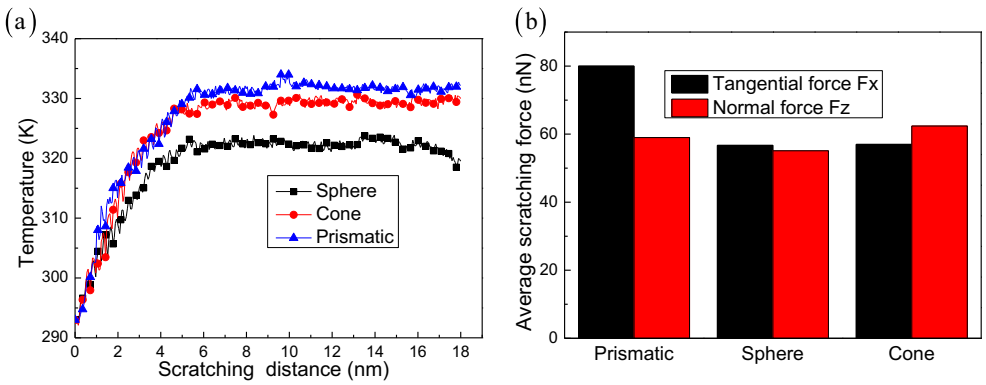

Fig. 15 Effect of tool shape **a** variation of the average temperature and **b** variations of scratching forces. (The depth of cut, tool speed, and surface roughness factors R_x and R_z are 1 nm, 30 m s^{-1}, and 1 and 0.3 nm, respectively)

different diamond tips with a contact area unequal. The increase of the number of workpiece atoms interacting with atoms at the front face of the tip intensifies the scratching force and depends on the tip shape.

Acknowledgments The authors would like to deeply appreciate the support from the NNSFC (11172094, 11372103, and 11172095), the NCET-11-0122, Hunan Provincial Natural Science Foundation for Creative Research Groups of China (12JJ7001), the Fok Ying-Tong Education Foundation, China (141005), the and Interdisciplinary Research Project of Hunan University.

References

1. Zhang LC, Biddut AQ, Ali YM (2010) Dependence of pad performance on its texture in polishing mono-crystalline silicon wafers. Int J Mech Sci 52:657–662
2. Xu W, Zhang LC, Wang X (2013) Laser bending of silicon sheet: absorption factor and mechanisms. J Manuf Sci Eng 135:061005–061011
3. Menezes PL, Kishore KSV (2006) Studies on friction and transfer layer: role of surface texture. Tribol Lett 24:265–273
4. Lee H, Bhushan B (2011) Role of surface roughness and lubricant film thickness in nano lubrication of sliding components in adaptive optics. J Colloid Interface Sci 353:574–581
5. Zhao WJ, Wang LP, Xue QJ (2010) Design and fabrication of nanopillar patterned Au textures for improving nanotribological performance. ACS Appl Mater Interfaces 2:788–794
6. Zhang X, Zhong X, Meng X, Yi G, Jia J (2012) Adhesion and friction studies of nano-textured surfaces produced by self-assembling Au nanoparticles on silicon wafers. Tribol Lett 46:65–73
7. Urbakh M, Klafter J, Gourdon D, Israelachvili J (2004) The nonlinear nature of friction. Nature 430:525–528
8. Wang H, Nair RP, Zou M, Larson PR, Pollack AL, Hobbs KL, Johnson Mathew Band Awitor OK (2007) Friction study of a Ni nanodot-patterned surface. Tribol Lett 28:183–189
9. Akarapu S, Sharp T, Robbins MO (2011) Stiffness of contacts between rough surfaces. Phys Rev Lett 106:204301–204304
10. Pohrt R, Popov VL (2012) Normal contact stiffness of elastic solids with fractal rough surfaces. Phys Rev Lett 108:104301–104304
11. Sharifi-Mood N, Koplik J, Maldarelli C (2013) Molecular dynamics simulation of the motion of colloidal nanoparticles in a solute concentration gradient and a comparison to the continuum limit. Phys Rev Lett 111:184501–184505
12. Zhou K, Nazarov AA, Wu MS (2007) Competing relaxation mechanisms in a disclinated nanowire: temperature and size effects. Phys Rev Lett 98:035501–035504
13. Zhou K, Nazarov AA, Wu MS (2006) Continuum and atomistic studies of a disclinated crack in a bicrystalline nanowire. Phys Rev B 73:045410–045410
14. Zhou K, Wu MS, Nazarov AA (2008) Relaxation of a disclinated tricrystalline nanowire. Acta Mater 56:5828–5836
15. Kuo CG, Chao CG (2007) A novel method of centrifugal processing for the synthesis of lead–bismuth eutectic alloy nanospheres and nanowires. Int J Adv Manuf Technol 32:468–472
16. Zhou K, Nazarov AA, Wu MS (2008) Atomistic simulations of the tensile strength of a disclinated bicrystalline nanofilm. Philos Mag 88:3181–3191
17. Zhang LC, Tanaka H (1997) Towards a deeper understanding of wear and friction on the atomic scale—a molecular dynamics analysis. Wear 211:44–53
18. Sun XZ, Cheng K (2010) Multi-scale simulation of the nano-metric cutting process. Int J Adv Manuf Technol 47:891–901
19. Zhu P, Hu Y, Fang F, Wang H (2012) Multiscale simulations of nanoindentation and nanoscratch of single crystal copper. Appl Surf Sci 258:4624–4631
20. Chen W, Liang Y, Luo X, Sun Y, Wang H (2014) Multi-scale surface simulation of the KDP crystal fly cutting machining. Int J Adv Manuf Technol 73:289–297
21. Tong Z, Liang Y, Jiang X (2014) An atomistic investigation on the mechanism of machining nanostructures when using single tip and multi-tip diamond tools. Appl Surf Sci 290:458–465
22. Tong Z, Liang Y, Yang X, Luo X (2014) Investigation on the thermal effects during nanometric cutting process while using nanoscale diamond tools. Int J Adv Manuf Technol:1–10
23. Xu W, Zhang LC (2014) On the mechanics and material removal mechanisms of vibration-assisted cutting of unidirectional fibre-reinforced polymer composites. Int J Mach Tools Manuf 80:1–10
24. Ji C, Shi J, Wang Y, Liu Z (2013) A numeric investigation of friction behaviors along tool/chip interface in nanometric machining of a single crystal copper structure. Int J Adv Manuf Technol 68:365–374
25. Han X, Gan YX (2013) Investigation the complex dynamic evolvement mechanism of particle cluster and surface integrity in the chemical mechanical planarization. Int J Adv Manuf Technol 64:13–22
26. Alao AR, Konneh M (2012) Surface finish prediction models for precision grinding of silicon. Int J Adv Manuf Technol 58:949–967
27. Zhang Z, Huo F, Wu Y, Huang H (2011) Precision grinding of silicon wafers using an ultrafine diamond wheel of a hybrid bond material. Int J Mach Tools Manuf 51:18–24
28. Zhang Z, Song Y, Xu C, Guo D (2012) A novel model for undeformed nanometer chips of soft-brittle HgCdTe films induced by ultrafine diamond grits. Scr Mater 67:197–200
29. Zhang Z, Xu C, Zhang X, Guo D (2012) Mechanical characteristics of nanocrystalline layers containing nanotwins induced by nanogrinding of soft-brittle CdZnTe single crystals. Scr Mater 67:392–395
30. Zhang Z, Huo F, Zhang X, Guo D (2012) Fabrication and size prediction of crystalline nanoparticles of silicon induced by nanogrinding with ultrafine diamond grits. Scr Mater 67:657–660
31. Chen Y, Zhang LC (2009) Polishing of polycrystalline diamond by the technique of dynamic friction part 4: establishing the polishing map. Int J Mach Tools Manuf 49:309–314
32. Chen Y, Zhang LC, Tang F (2012) Surface integrity of PCD composites generated by dynamic friction polishing: effect of processing conditions. Diam Relat Mater 26:25–31
33. Li J, Fang QH, Liu YW, Zhang LC (2014) A molecular dynamics investigation into the mechanisms of subsurface damage and material removal of monocrystalline copper subjected to nanoscale high speed grinding. Appl Surf Sci 303:331–343
34. Zhang Z, Zhang N, Ma G, Kang R (2013) Characterization of microstructural stability for nanotwinned mercury cadmium telluride under cyclic nanoindentations. Scr Mater 69:299–302
35. Zhang Z, Wang B, Zhang X (2014) A maximum in the hardness of nanotwinned cadmium telluride. Scr Mater 72:39–42
36. Foiles SM, Baskes MI, Daw MS (1986) Embedded-atom method functions for the fcc metals Cu Ag Au Ni Pd Pt and their alloys. Phys Rev B 33:7983–7991
37. Pei QX, Lu C, Lee HP (2007) Large scale molecular dynamics study of nanometric machining of copper. Comput Mater Sci 41:177–185
38. Zhang JJ, Sun T, Yan Y, Liang Y (2009) Molecular dynamics study of scratching velocity dependency in AFM-based nanometric scratching process. Mater Sci Eng A 505:65–69
39. Stadler J, Mikulla R, Trebin HR (1997) IMD: a software package for molecular dynamics studies on parallel computers. Int J Mod Phys C 8:1131–1140

40. Stukowski A (2010) Visualization and analysis of atomistic simulation data with OVITO—the Open Visualization Tool. Model Simul Mater Sci Eng 18:015012–015018
41. Zhang JJ, Hartmaier A, Wei YJ, Yan YD, Sun T (2013) Mechanisms of anisotropic friction in nanotwinned Cu revealed by atomistic simulations. Model Simul Mater Sci Eng 21:065001–065016
42. Ziegenhain G, Urbassek HM, Hartmaier A (2010) Influence of crystal anisotropy on elastic deformation and onset of plasticity in nanoindentation: a simulational study. J Appl Phys 107:061807–061807
43. Honeycutt JD, Andersen HC (1987) Molecular dynamics study of melting and freezing of small Lennard-Jones clusters. J Phys Chem 91:4950–4963
44. Huang JY, Ponce FA, Caldas PG, Prioli R, Almeida CM (2013) The effect of nanoscratching direction on the plastic deformation and surface morphology of InP crystals. J Appl Phys 114:203503–203511
45. Junge T, Molinari JF (2014) Plastic activity in nanoscratch molecular dynamics simulations of pure aluminium. Int J Plast 53:90–106
46. Tyrrell JW, Attard P (2001) Images of nanobubbles on hydrophobic surfaces and their interactions. Phys Rev Lett 87:176104–176107
47. Zhu PZ, Hu YZ, Ma TB, Wang H (2011) Molecular dynamics study on friction due to ploughing and adhesion in nanometric scratching process. Tribol Lett 41:41–46
48. Zhang P, Zhao H, Shi C, Zhang L, Huang H, Ren L (2013) Influence of double-tip scratch and single-tip scratch on nano-scratching process via molecular dynamics simulation. Appl Surf Sci 280:751–756
49. Fang TH, Weng CI, Chang JG (2002) Molecular dynamics simulation of nano-lithography process using atomic force microscopy. Surf Sci 501:138–147
50. Yan J, Zhang Z, Kuriyagawa T (2011) Effect of nanoparticle lubrication in diamond turning of reaction-bonded SiC. Int J Autom Technol 5:307–312
51. Tong Z, Liang Y, Jiang X, Luo X (2014) An atomistic investigation on the mechanism of machining nanostructures when using single tip and multi-tip diamond tools. Appl Surf Sci 290:458–465